PCCP

Accepted Manuscript

ROYAL SOCIETY OF CHEMISTRY

www.rsc.org/pccp

Operable persistent photoconductivity of Bi_2S_3 nested nano-networks

Ye Tian[a,b], Chuan Fei Guo[d], Jianming Zhang[c], and Qian Liu[a,e,]*

[a]National Center for Nanoscience and Technology (NCNST), China. No.11, Beiyitiao, Zhongguancun, 100190, China.
[b]The school of communication and electronics engineering, Hunan City University, Yiyang, Hunan, 413000, China.
[c]Suzhou Institute of Nano-tech and Nano-bionics (SINANO), Chinese Academy of Sciences, Suzhou, 212213, China.
[d]Department of Physics and TcSUH, University of Houston, Houston, TX 77204, USA
[e]Taida Applied Physics School, Nankai University, Tianjin 300457, China.

E-mail: liuq@nanoctr.cn

Keywords: Bi_2S_3, persistent photoconductivity, hierarchical nano-networks.

Recently, hierarchical nanostructures have attracted increasing attention because of their high specific surface area and abundant physical characteristics. Here we propose a hierarchical Bi_2S_3 nested nano-networks (Bi_2S_3-3N) with excellent thermally-stable lattice structure, which is prepared by topotactic transformation. Experimental results revealed that for the first time, Bi_2S_3-3N possesses an interesting nature of the repetitively-operable persistent photoconductivity, which is believed to stem from the releasing of photo-stimulated carriers captured by deep-level traps. This work shows great potential of topotactic transformed Bi_2S_3 hierarchical nanostructures in practical applications like functional porous nanoarchitectures, bistable optical-switching, photo detector, memory, *etc*.

1. Introduction

Hierarchical nanostructures have been paid increasing attention in recent years owing to their great potential in constructing novel nanodevices [1-6]. The large specific surface area of the hierarchical nanostructures is beneficial to many applications such as Li-ion battery, dye-sensitized solar cell, photo-catalyst, super-capacitor, light-emitting devices and hydrogen

storage [2, 4, 5, 7-15]. In the last decade, a variety of novel hierarchical nanostructures have been prepared by using different building blocks such as nanoparticles, nanoribbons, nanoplatelets, nanorods, nanodisks and so forth, [3, 16] based on a representative ''bottom-up'' assembly route. However, the assembly is limited due to non-uniform morphology and ability in mass production. In order to overcome these obstacles, sustaining efforts have been made in recent years [8, 16-19]. Very recently, topotactic transformation has been demonstrated to be a promising and general route to fabricate various hierarchical nanostructures, especially for bismuth (Bi) compounds with particular physical properties [8, 20-23].

Bi_2S_3 is a promising n-type semiconductor with many useable properties including photo catalysis, optical switching, solar energy, thermoelectricity, photoelectrochemistry, memristor, *etc*. [24-32]. Its carrier-traps related properties are relative less concerned since the traps often should be avoided in regular semiconductor materials[33, 34]. But the "needless" traps in ordinary situations are not always useless. Here we revealed that for the first time, Bi_2S_3 nested nano-networks (Bi_2S_3-3N) prepared by topotactic transformation exhibit a persistent photoconductance, which is believed to stem from the releasing of photo-stimulated carriers captured by deep level traps. Benefitting from the satisfying thermal stability of Bi_2S_3-3N, such operable persistent photoconductivity (PPC) shows the capability in cycle-switch the conductance of Bi_2S_3-3N between low and high level. Moreover, a surface treatment can further improve its operation speed.

2. Experimental Section

The raw material for the fabrication of Bi_2S_3-3N is the amorphous BiO_x thin film (thickness: 200 nm), which was deposited on glass substrate by reactive radio frequency (RF) magnetron sputtering (ULVAC, ACS-4000-C4) followed by thermal annealing in a muffle furnace at 400 °C for 3 hours for crystallization and then it was transformed to a β-Bi_2O_3 film. The thickness of the amorphous BiO_x thin film was measured by using a stylus profiler

(Vecco Dektak150). By simply immersing the β-Bi_2O_3 film into mixed solution of thioacetamide (TAA) and HCl (the concentration of HCl is 0.01-0.05 mol/L and that of TAA concentration is 0.01-0.1 mol/L, respectively), and incubating at 60 °C for 72 hours, the Bi_2S_3-3N was synthesized *via* topotactic transformation [8, 20-23, 35]. Morphology of the Bi_2S_3-3N was investigated by optical microscopy (OM, Olympus BX51-P microscope) and field-emission scanning electron microscopy (FE-SEM, Hitachi S-4800). The transmission electron microscopy (TEM), high resolution transmission electron microscopy (HR-TEM) observations and selective area electron diffraction (SAED) were performed with a field emission transmission electron microscope (FE-TEM, FEI Tecnai G^2 F-20) operating at an accelerating voltage of 200 kV. The temperature-dependent Raman spectra of the Bi_2S_3-3N was obtained with Raman Spectroscopy System (RENISHAW InVia Raman microscope) equipped with a heating stage. A continuous wave (CW) Argon laser (λ = 514 nm) was used as excitation light source and data collection ranges from 100 to 800 cm^{-1}.

A typical Bi_2S_3-3N film used to study persistent photoconductivitywas prepared in a mixture solution of TAA with a concentration (C_{TAA}=0.05 $molL^{-1}$) and HCl with a concentration (C_{HCl}=0.04 $molL^{-1}$) [23], because it can provide a larger specific surface area compared with other Bi_2S_3-3N films obtained with different reagent concentrations (Supporting information 1). The silver paste with a typical size of 1 mm is used to prepare the electrodes on Bi_2S_3-3N for photoconductivity study, and the geometric distance between two electrodes is 10 mm. The electrical/opt-electrical properties are tested by Keithley 2635A source meter and semiconductor laser diode with a wavelength of 671 nm, whose power density can be tuned by control the current through the diode. The contact angle of the sample is evaluated by contact angle test (Kruss DSA100).

3. Results and discussions

3.1 The topotactic transformation from β-Bi_2O_3 to Bi_2S_3-3N

The topotactic transformations *via* the epitaxial growth utilizing the lattice match among β-Bi_2O_3, BiOX (X=Cl, Br, I) and Bi_2S_3 (*e.g.*, the lattice misfits of (100) plane of BiOCl and (001) plane Bi_2S_3 in reference to (200) plane of β-Bi_2O_3 is 0.43% and 2.4% as presented in Ref. [22, 36]) have been successfully demonstrated that the networks structures of Bi_2S_3 like Bi_2S_3-3N can be prepared [8, 21, 22, 37]. In our case, the transformation is a combination of two processes as shown in Figure 1a: the fast transformation (less than 2 min) in the solution containing HCl from β-Bi_2O_3 domain to the 2D networks of BiOCl nanoplates, which is induced by the wet-etching of β-Bi_2O_3, together with the following hydrolyzation of $BiCl_3$ [20]:

$$A: Bi_2O_3+6HCl \rightarrow 2\ BiCl_3+3H_2O,$$

$$B: 2BiCl_3+2H_2O \rightarrow 2\ BiOCl+4HCl.$$

And then the slow epitaxial growth (~72 h) of nested networks of Bi_2S_3 nanorods on the surface of BiOCl [23]. In this process,the BiOCl nanosheets are sulfurized, in which O and Cl are completely replaced by S^{2-} released from TAA in the acid environment, and form interwoven single-crystalline nanorods of Bi_2S_3due to its solubility [23]. Very recently, it was discovered that the sulfurization process could be shorten to 5 h by thiourea *using* solvothermal reaction [36], enabling us to carried out the topotactic transformation to Bi_2S_3-3N more effectively. The OM and low-magnification FE-SEM images shown in Figure 1b and 1c confirm that all the domains are made of order-arranged nanoplates. High-magnification SEM image and corresponding Fast Fourier transformation (FFT) pattern in Figure 1d indicate that nanoplates are orthogonally arranged with an average length of about 1 μm and a thickness of 20 nm, while high-magnification image in Figure 1e shows that the plates are in fact nano-networks made of interwoven nanorods.

3.2. Operable persistent photoconductivity in the Bi_2S_3-3N

A sample used for testing photocurrent is showed in Figure 2. Here the Bi_2S_3-3N film is first prepared on a glass substrate, and then two ohmic-contacted electrodes are built on two sides of the film using silver paste (blue data in the inset of Figure 2). When a 671 nm laser diode (power density=14.8 mW/cm^2) irradiates the film, electrons would be excited directly from the valance band to the conductance band because the photon energy (1.85 eV) is larger than the band gap of Bi_2S_3-3N (~1.42 eV, extracted from Tuac-plot of the absorption spectra, Supporting information 1). Consequently, the photocurrent appears (Figure 2) [26, 28, 30, 31, 38]. However, unlike other Bi_2S_3 nanostructures with relatively fast photoconductive response [25, 31], the photocurrent of the Bi_2S_3-3N takes a longer time (~100 s) to reach the stable plateau (Figure 2). This might be ascribed to the surface-related slow process produced by amounts of surface traps on the Bi_2S_3-3N with large specific surface area [39]. It is known that the trapping could hinder the carriers take part in the current-transport [33, 34], and thus in our case the rise of the photocurrent mainly contributed by the considerable carriers photo-exited on huge surface of the Bi_2S_3-3N would be slow down remarkably. Likewise, the current drops quite slowly after the laser is turned off, and does not decrease to the initial value (Figure 2), showing a typical persistent photoconductivity (PPC) phenomenon [29, 40-43]. The PPC is closely related to the carrier traps [29, 40-43], and the large specific surface area of Bi_2S_3-3N may lead to more surface traps [39], resulting in the slow-decrease of the photocurrent. The photocurrent linearly depends on the power density (red data in the inset of Figure 2 and supporting information 2), implying that the heat produced by the illumination is quite weak in these cases, and thus do not induce thermal-saturation of the photo-stimulated carriers [44]. Hence in our studied range, the PPC behavior is almost not affected by the power density.

Basically, the drop of the photo-current is induced by the recombination of electrons and holes, which is eminently affected by the carrier-traps as well as its energy level. For the traps whose energy levels are shallow, the electrons can easily escape from these traps and then recombine with the hole in the valance band, whereas for deep-energy-level traps, captured

electrons are difficult to escape and recombine with the holes. Since the current transport in the semiconductors contains the contribution from both electrons and holes, and they recombine in pairs [44], the fact that there are electrons captured in the deep traps implies that considerable holes might be not recombined by the electrons (captured in deep traps), thus contribute to the current transport and produce a stable/metastable conductance [27,28]. This is a well-known insight of the PPC effect [40]. The energy-level-dependence of the trap-related recombination implies that the kinetics of the photo-current relaxation may provide valuable information about the energy distribution of the traps, which should be helpful for us to further understand the PPC in the Bi_2S_3-3N system. Here the decay of the photo-current follows the stretched exponential model [43]:

$$I = I_0 \exp[-(t/\tau)^{\beta}] \quad (1)$$

where I_0 is the current at the onset of decay, β ($0<\beta<1$) is a parameter reflecting the distribution of traps that control the decay process, and τ is a feature time. The β and τ extracted by fitting Eq. (1) is 0.15 and 295.6 s, respectively (green line in Figure 4), predicting a recovery time of months. A rather small β indicates that the energy levels of traps have a broad distribution around the conductance band[40, 43]. *i.e.*, besides the shallow traps, also considerable deep traps exist in Bi_2S_3-3N, resulting in its PPC phenomenon [40].

It is interesting to explore how to release the stable-trapped carriers. To some extent, if we take the switching from the initial low conductance state to the metastable conductance state as the "writing" operation, the release of the trapped carriers would correspond to an "erasing" operation. That is to say, the Bi_2S_3-3N may work something like a memory. Usually, the traps are deemed as the localized states in the band gap, and the localized (trapped) carrier can move with the assistance of the phonons [44]. Therefore, a simple manner to release the carriers is to increase the energy and density of the phonons in the sample by heating [44, 45]. Heating can make the trapped carriers more active, thus prompting the recombination. As

shown in Figure 2, after heating the sample to 350 K, the trapped carriers are fully released (erase the memory). Considering the thermal-stability of Bi_2S_3-3N (discussed latter), it is safe to use the Bi_2S_3-3N memory under 350 K with "optical-writing", "electrical-reading" and "thermal-erasing", as shown in right-bottom of Figure 2. Although its operation speed is still unsatisfying, in compare with purely optical- (compact disc (CD), digital versatile disc (DVD), etc.) or electrical- (dynamic random access memory (DRAM), static random access memory (SRAM), Flash, etc.) memory widely used nowadays, such optical-electrical-hybrid memory might be useful to merge the optical information processing system and electrical information processing system. *e.g.*, the information transported via an optical-waveguide can be directly transferred to the conductance level by such operable PPC and become direct-readable by an electrical circuit.

To further ensure the "erase" is a thermal effect other than the photo or electrical effect demonstrated in some other systems[45-47], the influence of these two factors should be checked. We found the device could be kept at the metastable high conductance state under multi-illuminations (supporting information 2), indicating the 671 nm laser itself could not directly switch the device back to initial dark state. This is because its photo energy mismatches the energy to photo-stimulate the trapped carriers, which is often smaller than the band gap[46]. And the heat effect of the illumination is also weak as mentioned above. Therefore the "erase" is almost impossible to be induced by photo-thermal effect. On the other hand, the electrical erase had ever been carried out successfully in field effect transistor (FET) type device *via* the external gate bias which could produce equivalent high field intensity of ~10^8 V/m vertical to the current channel [45, 47]. However, in our two-electrode device, the electrical field built along the current channel is ~10^2 V/m, far lower than the field intensity needed to draft the carriers out of the traps and result in the variation of the conductance ("erase"). By studying the temporal evolution of the dark current, we estimated that the conductance decay induced by the bias voltage even in long-term is just 0.46%

(supporting information 3). Hence the contribution of the electrical effect to the erase is also quite low.

3.2. Surface treatment to improve manipulation speed

The prototype device with "optical-writing", "electrical-reading" and "thermal-erasing" based on the Bi_2S_3-3N successfully shows that it can serve as a re-writable memory. However, to a large extent, the device has a disadvantage of the long operation time in thermal release (~1400 s), which is not practically useful. Considering the nature of the carriers traps in the Bi_2S_3-3N, surface treatment might be an alterable route to accelerate the release. Here the methanol is a suitable selection, because it can passivate the deep traps, thus is beneficial to release of captured electrons and accelerates the recombination [25]. As a result, the "erasing" would become easier and faster. Moreover, since the methanol is volatile, the Bi_2S_3-3N could return to its initial state without any methanol leftovers on its surface, and thus the cyclic writing-reading-erasing operation is possible. Figure 3a shows that when the methanol is dipped on the surface of the Bi_2S_3-3N which has been optically switched to metastable high conductance state, its current steeply increases firstly with the spread of the methanol because the conductance of the Bi_2S_3-3N covered by methanol is observably higher than that in air (supporting information 4), corresponding to the start time point (C point) of the sharp growth of dI/dt in Figure 3b. Afterward, once the methanol evaporates, the current drops to the initial dark level (I_D), and $dI/dt \rightarrow 0$ (D point, Figure 3a and 3b), indicating that the recombination accelerated by methanol treatment could be carried out in a time much shorter than aforementioned "thermal-erase" and mainly determined by the mean duration of the methanol evaporation (13.6±3 s, statistics to five cycles shown in Figure. 2b, supporting information 4). This means that the "erasing" time in this case is squeezed to ~1/103 of the thermal approach. Meanwhile, benefiting to the good volatile ability of the methanol, the "Erase" to the surface treated device can be well repeatable: the dark current and the current at metastable high

conductance state during the cycles fluctuates around 145.9 nA (Fig. 2, statistics to 435 values of the dark current) and 163.7 nA (Fig. 2, statistics to the currents in all five cycles) with a relative standard deviations of 3.9% and 2.5%, respectively, in the whole measurement without any overlap which probably produces the error to recognize the conductance state. Schematically, the critical role of the methanol absorbed on the surface of Bi_2S_3-3N is illustrated in Figure 3c: when the Bi_2S_3-3N is illuminated by 671 nm laser, the electrons would be excited from valence band to conductance band. Accordingly, equal amount of holes generates in valence band. And almost spontaneously, the traps start to capture the excited electrons (1→2). When the light is turned off, the free (on conductance band) and releasable (in shadow traps) electrons would recombine with the holes in pairs, but the electrons in deep traps are difficult to be recombined. Consequently, the remaining holes induce the PPC phenomenon (2→3). Once the methanol is dipped on the Bi_2S_3-3N and passivates its traps, the trapped electrons would become easy to release (3→4), and thus complete the recombination with the holes. Hence Bi_2S_3-3N can be switched back (erased) to initial state (4→1).

To study whether such methanol-based passivation is extendable, it is significant to test the "erase" effect of other surface-chemical approaches, and the alcohol might be the most natural choice to check the potential extendibility. However, alcohol treatment can distroy the network-structure of the Bi_2S_3-3N because alcohol chelates with bismuth compounds and thus would form metal-organic complexes [25] (supporting inforamtation 5). Therefore, erasing *via* alcohol is not viable. Even though, existing works still imply that the alcohols could be a sound passivator to the surface traps of other metal sulfides (if not chelated with the alcohol) [48, 49]. *e.g.*, the alcohol could fill the empty surface state (surface passivation) of ZnS quantum dot and enhance its photoluminescence [49]. On the other hand, it is found that that the sample with small contact angle is beneficial to obtain a quick "erasing": Compared with the sample aforementioned with small contact angle (supporting information 5), the duration of the

"erasing" of the sample with larger contact angle becomes longer (supporting information 5). This is because the small contact angle indicates that the sample has a lower surface energy, which enable the methanol to sprawl swiftly [50], and thus level up the "erasing" speed. Therefore we may further shorten the "erasing" time by preparing the samples with smaller contact angle. Of course, the carriers in traps are also possible to be released through other manners such as high electrical field provided by external gate bias voltage if the device structure could be upgraded from two-electrode type to FET type. And the light-illumination with suitable wavelength is also accessible[45-47], providing us more choices to erase much faster and conveniently.

3.3. The structure origin of the traps in the Bi_2S_3-3N

As discussed above, considerable carrier traps existing in the surface of the Bi_2S_3-3N is believed to be the origin of the PPC effect which is operable. However, further evidences are needed to confirm the existence of the traps. Since the traps are often closely related to the lattice defects of the material, detail characterizations to the crystal structure of the Bi_2S_3-3N are carried out. The selected area electron diffraction (SAED) pattern of an entire Bi_2S_3-3N plate shown in the inset of Figure 4a exhibits bright spots with a tetragonal symmetry, indicating that the perpendicularly-aligned nanorods are a good crystal structure with vertically interwoven. Actually, the diffraction spots are a combination of two sets of patterns (α and β) with a 90 ° intersection angle. According to the previous reports[8, 23], these nanorods grow along the [001] direction, and the four tetragonally arranged strong spots are corresponding to the (002) planes of the orthorhombic Bi_2S_3 with a *d*-spacing of 1.99 Å, as shown in Figure 4a. Additionally, the clear lattice fringes in high resolution transmission electron microscopy (HR-TEM) image further indicate the good crystallinity of the Bi_2S_3-3N (Figure 4b) plates. However, it is worth noting that there are surface defects which might be formed when exposed in air, and this might explain that there are some stray spots in the

SAED pattern as well as an amorphous layer on the surfaces of the rods in HR-TEM image. Figures 4c and 4d show the normal and dark field TEM images for the same region of Bi_2S_3-3N, visualizing the spatial distribution of the defect clouds on the surface of the nanorods, which may have surface carrier-traps producing the PPC of the Bi_2S_3-3N. Considering that the Bi_2S_3 is derived from Bi_2O_3, a possible chemical origin of the traps might be the residual oxygen. As we known, sulfur and oxygen are two elements belonging to the same group, thus oxygen is possible to occupy the site of sulfur and induce lattice distortion, resulting in the traps in Bi_2S_3-3N. Even though, further investigations are still necessary to uncover the issue.

3.4. The stability of the Bi_2S_3-3N

For the hierarchical nanostructures, the endurance is especially critical to the structural stability. Here the lattice structure stability of the products was studied by the temperature-dependent Raman spectra (Figure 5a). There are two Raman bands at 238.2 cm^{-1} with a full width at half maximum (FWHM) of 37 cm^{-1}, and 260.9 cm^{-1} with a FWHM of 18 cm^{-1}, which are consistent well with the results of rod-like Bi_2S_3 [32]. The large FWHMs are related to the small size of the nanorods, which breaks the crystalline-symmetry and results in the broad Raman bands [20]. The bands become even wider when heated from 300 K to 500 K, and can return to the original width when cooled down. Such revertible variation of the spectra indicates that the crystal structure of the Bi_2S_3-3N is stable during the thermal treatment. Moreover, the Bi_2S_3-3N samples annealed at different temperatures (300 K, 400 K and 500 K) for 30 min are observed by TEM as shown in Figure 5b-d. From their SAED patterns, no apparent variation is observed in the lattice structures, further confirming the thermal stability of the crystal structure of the Bi_2S_3-3N. Surface oxidation is another potential factor producing variation of the lattice structure. Our previous work shows that the typical temperature at which Bi_2S_3-3N is apparently oxidized to Bi_2O_3 is 593K (320 ^oC). Hence the

oxidation of Bi_2S_3-3N at its operation temperature (<350 K) should be not severe to change the PPC as well as its erasure behaviors. Therefore it can conclude that the PPC of the Bi_2S_3-3N is safe to be operated under 350 K with "optical-writing", "electrical-reading" and "thermal-erasing", as shown in right-bottom of Figure 1e.

4. Conclusion

In summery, the nested nano-networks of Bi_2S_3 were synthesized by using topotactic transformations. Base on the variable temperature Raman spectra and TEM observation, high thermal-stability of the crystal structure is verified up to 500 K. The topotactic-transformed Bi_2S_3 nested nano-network shows persistent photoconductivity, which stems from the carriers with the metastable traps. Through a hybridized strategy combining "optical-write", "electrical-reading" and "thermal-erasing", the PPC of Bi_2S_3-3N can be operated repeatedly. And its operation speed could be increased by surface treatment using methanol. In addition, the PPC of Bi_2S_3-3N can be applied to optical switch. Our investigation in the properties of the Bi_2S_3-3N with topotactic-transformed hierarchical nanostructures may result in potential application in constructing novel nanodevices.

Acknowledgements

This work was supported by the National Natural Science Foundation of China (11374069), the Chinese Academy of Sciences Strategic Pilot Program (XDA09020300), the National Basic Research Program of China (2010CB934102), and the Natural Science Foundation of Hunan province (2015JJ6015).

References

1. Y. Chen, C. Zhu, X. Shi, M. Cao and H. Jin, *Nanotechnology*, 2008, **19**, 205603.
2. C. Cheng, B. Liu, H. Yang, W. Zhou, L. Sun, R. Chen, S. F. Yu, J. Zhang, H. Gong and H. Sun, *Acs Nano*, 2009, **3**, 3069-3076.
3. Y. Huang, X. Duan, Q. Wei and C. M. Lieber, *Science*, 2001, **291**, 630-633.
4. Q. Ke, C. Tang, Y. Liu, H. Liu and J. Wang, *Materials Research Express*, 2014, **1**, 025015.
5. I. López, E. Nogales, B. Méndez, J. Piqueras, A. Castaldini and A. Cavallini, *Materials Research Express*, 2014, **1**, 025017.

6. X. Xia, Y. Zhang, D. Chao, C. Guan, Y. Zhang, L. Li, X. Ge, I. M. Bacho, J. Tu and H. J. Fan, *Nanoscale*, 2014, **6**, 5008-5048.
7. S. H. Ko, D. Lee, H. W. Kang, K. H. Nam, J. Y. Yeo, S. J. Hong, C. P. Grigoropoulos and H. J. Sung, *Nano letters*, 2011, **11**, 666-671.
8. L. Li, N. Sun, Y. Huang, Y. Qin, N. Zhao, J. Gao, M. Li, H. Zhou and L. Qi, *Advanced Functional Materials*, 2008, **18**, 1194-1201.
9. Q. Li, R. Jiang, Y. Dou, Z. Wu, T. Huang, D. Feng, J. Yang, A. Yu and D. Zhao, *Carbon*, 2011, **49**, 1248-1257.
10. X. Wang, J. C. Yu, C. Ho, Y. Hou and X. Fu, *Langmuir*, 2005, **21**, 2552-2559.
11. X. M. Yin, C. C. Li, M. Zhang, Q. Y. Hao, S. Liu, L. B. Chen and T. H. Wang, *The Journal of Physical Chemistry C*, 2010, **114**, 8084-8088.
12. J. Luo, X. Xia, Y. Luo, C. Guan, J. Liu, X. Qi, C. F. Ng, T. Yu, H. Zhang and H. J. Fan, *Advanced Energy Materials*, 2013, **3**, 737-743.
13. S. K. Karuturi, J. Luo, C. Cheng, L. Liu, L. T. Su, A. I. Y. Tok and H. J. Fan, *Advanced Materials*, 2012, **24**, 4157-4162.
14. J. Liu, Z. Guo, W. Wang, Q. Huang, K. Zhu and X. Chen, *Nanoscale*, 2011, **3**, 1470-1473.
15. W. Wang, Q. Zhao, K. Laurent, Y. Leprince-Wang, Z.-M. Liao and D. Yu, *Nanoscale*, 2012, **4**, 261-268.
16. J. A. Elemans, A. E. Rowan and R. J. Nolte, *Journal of Materials Chemistry*, 2003, **13**, 2661-2670.
17. Y. Lin, A. Böker, J. He, K. Sill, H. Xiang, C. Abetz, X. Li, J. Wang, T. Emrick and S. Long, *Nature*, 2005, **434**, 55-59.
18. Z. Li, X. Wei, T. Ming, J. Wang and T. Ngai, *Chemical Communications*, 2010, **46**, 8767-8769.
19. L.-Y. Pan, Y.-L. Zhang, H.-Y. Wang, H. Liu, J.-S. Luo, H. Xia, L. Zhao, Q.-D. Chen, S.-P. Xu, B.-R. Gao, L.-M. Fu and H.-B. Sun, *Nanoscale*, 2011, **3**, 2882-2888.
20. Y. Tian, C. F. Guo, Y. Guo, Q. Wang and Q. Liu, *Applied Surface Science*, 2012, **258**, 1949-1954.
21. C. F. Guo, J. Zhang, M. Wang, Y. Tian and Q. Liu, *Small*, 2013.
22. C. F. Guo, J. Zhang, Y. Tian and Q. Liu, *ACS nano*, 2012, **6**, 8746-8752.
23. C. F. Guo, S. Cao, J. Zhang, H. Tang, S. Guo, Y. Tian and Q. Liu, *Journal of the American Chemical Society*, 2011, **133**, 8211-8215.
24. Y. Tian, C. F. Guo, S. Guo, T. F. Yu and Q. Liu, *Nano Research*, **7**, 9.
25. G. Konstantatos, L. Levina, J. Tang and E. H. Sargent, *Nano letters*, 2008, **8**, 4002-4006.
26. A. A. Tahir, M. A. Ehsan, M. Mazhar, K. U. Wijayantha, M. Zeller and A. Hunter, *Chemistry of Materials*, 2010, **22**, 5084-5092.
27. C. Song, D. Wang, T. Yang and Z. Hu, *CrystEngComm*, 2011, **13**, 3087-3092.
28. Z.-H. Ge, B.-P. Zhang, P.-P. Shang, Y.-Q. Yu, C. Chen and J.-F. Li, *Journal of electronic materials*, 2011, **40**, 1087-1094.
29. R. Bhattacharya and P. Pramanik, *Journal of The Electrochemical Society*, 1982, **129**, 332-335.
30. T. Wu, X. Zhou, H. Zhang and X. Zhong, *Nano Research*, 2010, **3**, 379-386.
31. H. Bao, C. M. Li, X. Cui, Q. Song, H. Yang and J. Guo, *Nanotechnology*, 2008, **19**, 335302.
32. Y. Xiao, H. Cao, K. Liu, S. Zhang and V. Chernow, *Nanotechnology*, 2010, **21**, 145601.
33. j. shen and j. yang, *j. appl. phys*, 2008, 7706-7714.
34. a. kumar, m. v. fischetti, t. h. ning and e. gusev, *journal of applied physics*, 2003, **94**.

35. Y. Tian, L. Jiang, X. Zhang, Y. Deng and S. Deng, *Materials Research Express*, 2014, **1**, 035034.
36. H. Yu, H. Bao, K. Zhao, Z. Du, H. Zhang and X. Zhong, *the journal of physical chemistry c*, 2014, online.
37. J. Zhang, C. Guo, Y. Tian and Q. Liu, *chinese science bulletin*, 2014.
38. R. Vogel, P. Hoyer and H. Weller, *The Journal of Physical Chemistry*, 1994, **98**, 3183-3188.
39. P. Sharma, K. Sreenivas and K. V. Rao, *Journal of Applied Physics*, 2003, **93**, 3963-3970.
40. C. H. Qiu and J. Pankove, *Applied physics letters*, 1997, **70**, 1983-1985.
41. G. Yusa and H. Sakaki, *Applied physics letters*, 1997, **70**, 345-347.
42. D. Lang and R. Logan, *Physical Review Letters*, 1977, **39**, 635.
43. J. Reemts and A. Kittel, *Journal of applied physics*, 2007, **101**, 013709-013709-013705.
44. S. M. Sze and K. K. Ng, *Physics of semiconductor devices*, Wiley. com, 2006.
45. K. Ghaffarzadeh, A. Nathan, J. Robertson, S. Kim, S. Jeon, C. Kim, U.-I. Chung and J.-H. Lee, *Applied Physics Letters*, 2010, **97**, 143510-143510-143513.
46. Y. Wang, Z. Liao, G. She, L. Mu, D. Chen and W. Shi, *Applied Physics Letters*, 2011, **98**, 203108-203108-203103.
47. S. Jeon, S.-E. Ahn, I. Song, C. J. Kim, U.-I. Chung, E. Lee, I. Yoo, A. Nathan, S. Lee and J. Robertson, *Nature materials*, 2012, **11**, 301-305.
48. A. Datta, S. K. Panda and S. Chaudhuri, *The Journal of Physical Chemistry C*, 2007, **111**, 17260-17264.
49. L. Sun, C. Yan, C. Liu, C. Liao, D. Li and J. Yu, *Journal of alloys and compounds*, 1998, **275**, 234-237.
50. y. fang, g. sun, q. cong, g.-h. chen and l.-q. ren, *jornal of bon ngnrng*, 2008, 127-133.

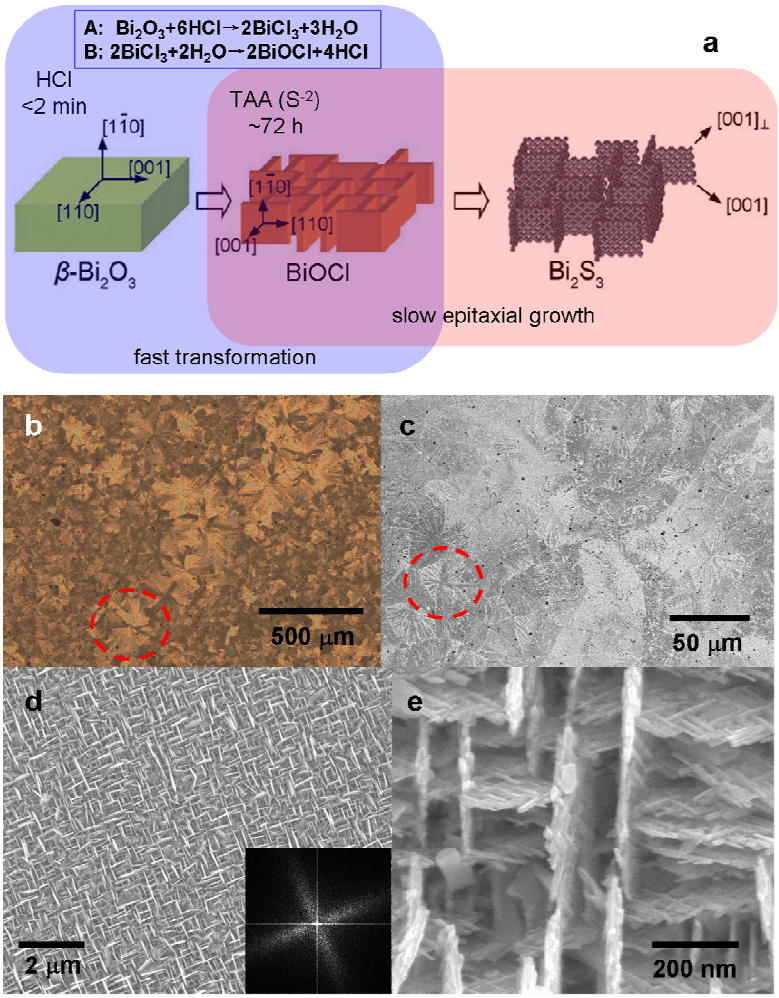

Figure 1. (a) Topotactic transformation process from β-Bi_2O_3 to Bi_2S_3-3N; (b) OM and (c) low magnified SEM image of the Bi_2S_3-3N consist of domains; (d) the SEM image of single Bi_2S_3-3N domain constructed with orthogonal-arranged nanoplates and its Fourier transformation pattern; (e) SEM image of the Bi_2S_3 nanoplates consisting of interwoven nanorods.

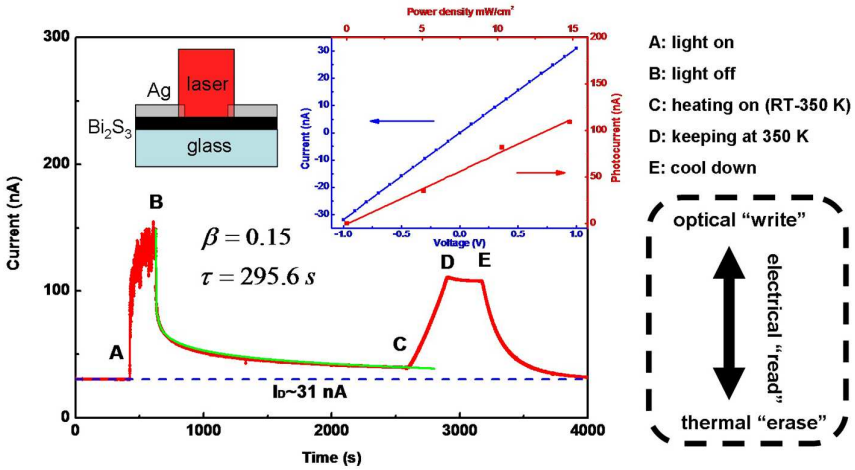

Figure 2. (a) PPC behavior of the Bi_2S_3-3N, the thermal release of the metastable high conductive state and induced hybridized storage strategy combining "optical-writing", "electrical-reading" and "thermal-erasing".

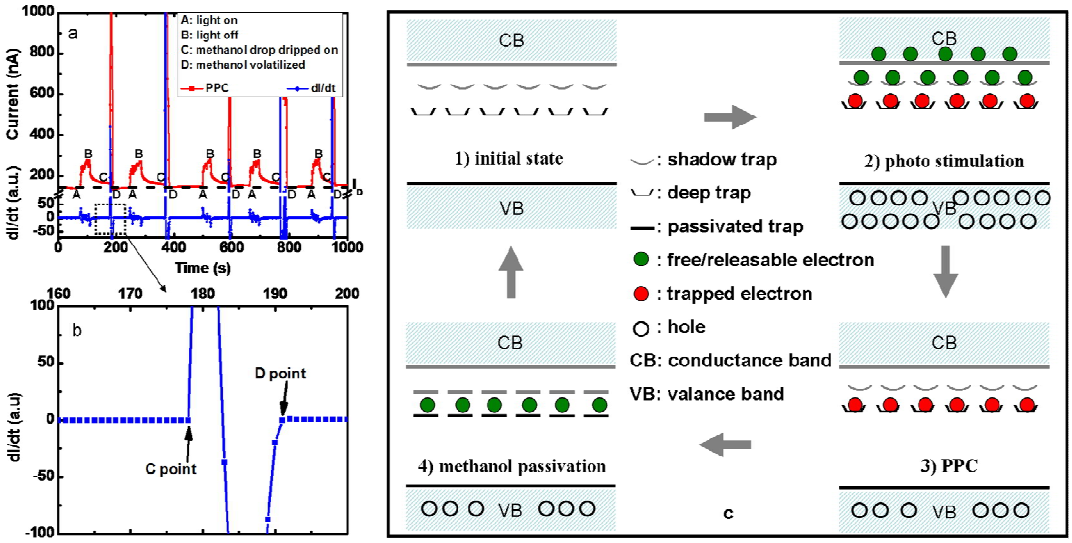

Figure 3. (a) Surface-treatment-enhanced operation speed to the PPC of the Bi_2S_3-3N; (b) Enlarged image shown the detail of dI/dt in the process from the dipping to the evaporation of methanol; (c) schematically illustration to the mechanism of methanol-operation of PPC.

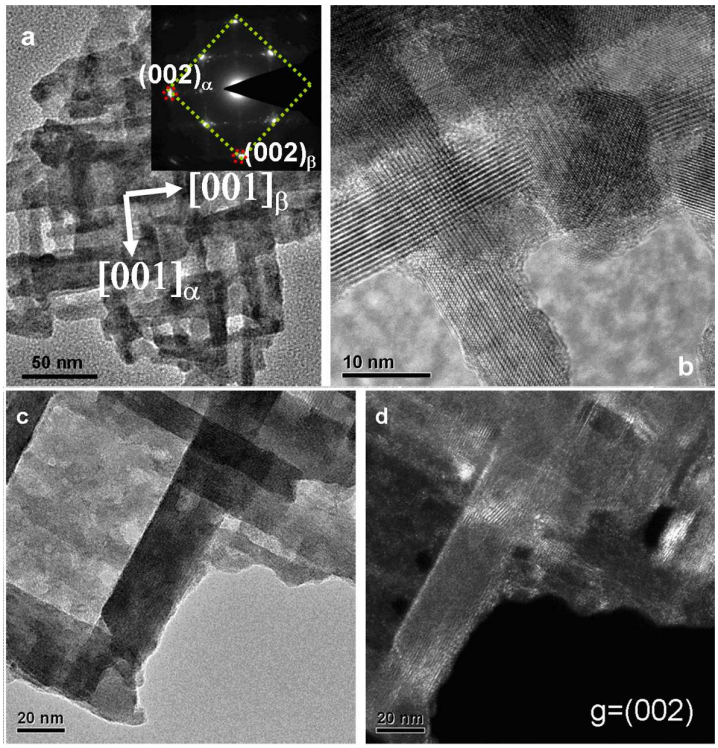

Figure 4. (a) Low magnification TEM image and corresponding SAED patterns of the Bi_2S_3-3N; (b) HRTEM image of the Bi_2S_3-3N; (c) normal and (d) dark field TEM image for a same area in the Bi_2S_3-3N visualizes the spatial distribution of the defects.

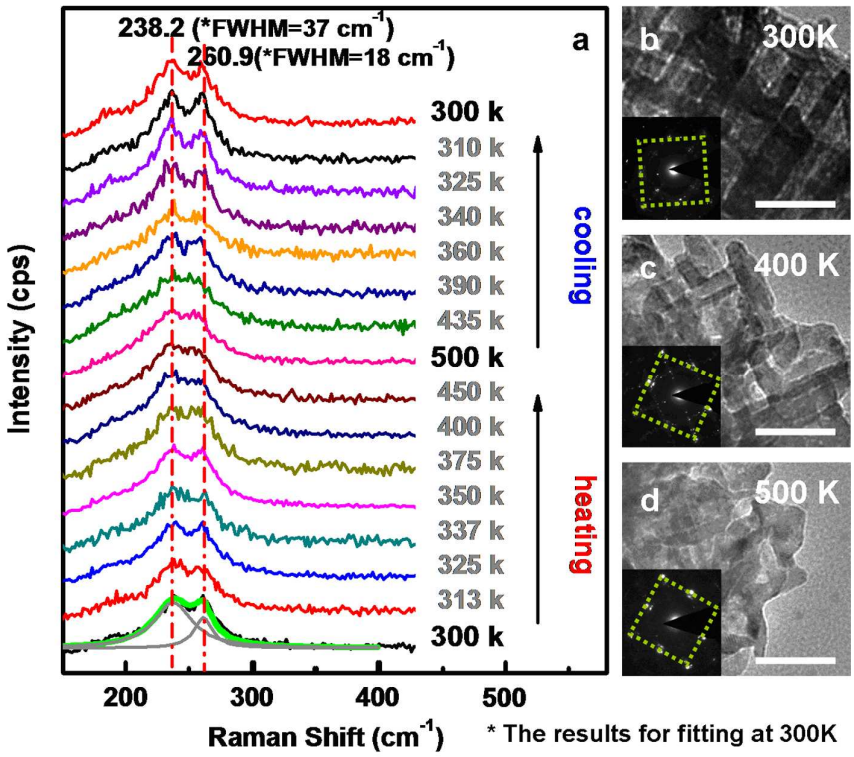

Figure 5. (a) Temperature-dependent Raman spectra of the Bi_2S_3-3N (300 -500-300K). Low magnification TEM images and corresponding SAED patterns of the Bi_2S_3-3N after heated under (b) 300 K, (c) 400 K and (d) 500 K. The scale bar in these images is 50 nm.